IIETA International Information and Engineering Technology Association
Advancing the World of Information and Engineering

Annales de Chimie - Science des Matériaux
Vol. 49, No. 6, December, 2025, pp. 601-614
Journal homepage: http://iieta.org/journals/acsm

Thermo-Mechanical Characterization of Gypsum–Nano Silica Modified Fired Clay Bricks at Elevated Temperatures

Abbas Fadhil Shannoon

Geniuses High School for Outstanding Students, The General Directorate Al-Rusafa the Third, Ministry of Education, Baghdad 10059, Iraq

Corresponding Author Email: knanybas71@gmail.com

https://doi.org/10.18280/acsm.490603

Received: 3 November 2025
Revised: 12 December 2025
Accepted: 20 December 2025
Available online: 31 December 2025

Keywords:
fired clay bricks, nano-silica, gypsum, thermo-mechanical properties, Fourier transform infrared spectroscopy analysis

ABSTRACT

The current research aims to develop fired clay bricks with gypsum and nanosilica from rice straw as additives to improve the thermomechanical properties of conventional clay bricks. Laboratory-based clay brick samples were prepared by adding commercial gypsum (G) at 0% and 5%, nanosilica (S) prepared from rice straw waste materials at 0%, 5%, and 10% proportions, and firing at temperatures of 900, 1000, and 1100°C. The mineral and phase transformations of prepared nanosilica and brick samples were investigated using X-ray diffraction (XRD), X-ray fluorescence (XRF), thermogravimetric analysis–derivative differential thermal analysis (TGA-drDTA), and scanning electron microscopy with energy-dispersive X-ray spectroscopy (SEM–EDS) techniques. Properties were compared to those of conventional bricks that did not contain additives. Synthesized nanosilica was found to be 127 nm and suitable as an additive. The results of the fireclay bricks with gypsum and nanosilica additives indicate that increasing the silicate polymerization and glaze phase formation from 25% to 45% reduces the microcracking density from 4.4 to 2.8 cracks/mm² at 1100°C, with a composition of G5%-S10%. Reduce compressive strength (from 35 to 12.8 MPa), water absorption capacity (18.6 to 13.6%), and thermal conductivity (0.28-0.76 W/m.K) to meet ASTM requirements. Finally, it was concluded that the addition of gypsum and nanosilica additive improves the thermochemical stability and mechanical properties of fired clay bricks, making them suitable for energy-efficient and fire-safe construction materials.

1. INTRODUCTION

Bricks are a well-known and essential building material in Iraqi society and across many developing regions. Traditionally, bricks are produced from clay that is shaped, dried, and fired at high temperatures until sufficient strength and durability are achieved [1]. Depending on performance requirements, brick bodies may consist of pure clay or clay blended with supplementary materials. However, conventional compositions do not always meet modern structural and thermal demands. For instance, unfired bricks incorporating sodium hydroxide and sodium silicate have shown relatively low compressive strength values of 1.048–1.28 MPa, which limits their structural applicability [2].

In recent years, growing attention has been directed toward the use of waste additives and waste-derived nanomaterials in brick production, primarily for sustainability and performance enhancement. Several studies have reported that waste-based nanosilica can be effectively reintroduced into ceramic matrices, leading to improvements in physical, mechanical, and thermal properties [3-7]. Advanced characterization techniques such as X-ray diffraction (XRD), scanning electron microscopy with energy-dispersive X-ray spectroscopy (SEM–EDS), X-ray fluorescence (XRF), and thermogravimetric analysis (TGA) now allow more precise evaluation of mineralogical and microstructural changes, although the complex physicochemical behavior of clay-based systems is still not fully understood [8]. Literature surveys consistently indicate that nanomaterial additives enhance thermochemical stability and mechanical performance in clay ceramics [8-11].

Among available nanomaterials, nanosilica is particularly attractive due to its high surface area, pozzolanic activity, and microstructure-refining capability. Gypsum, on the other hand, is an abundant and low-cost calcium-based mineral known to influence hydration behavior, phase transformations, and thermal cracking resistance in clay composites [8]. Yet, despite these advantages, the combined effect of gypsum and nanosilica in fired clay bricks—especially under elevated temperatures—remains insufficiently explored. Similar observations have been reported for other nanomodified systems, such as TiO_2-containing mortars, where density reduction, increased porosity, and shrinkage were observed [12]. Research on such modified bricks at high temperatures is still limited [13].

This clear research gap highlights the need for a systematic

investigation into the thermal and mechanical response of gypsum–nanosilica-modified fired bricks. Accordingly, the present study aims to develop clay-based fired bricks incorporating gypsum and agricultural waste-derived nanosilica, sintered between 900 and 1100℃. The novelty lies in evaluating their coupled thermomechanical performance and phase evolution using comprehensive material characterization techniques, thereby contributing to safer and more energy-efficient construction materials.

2. MATERIALS AND METHODS

Materials: All the chemicals used in the study purchased from Sigma Aldrich, India, Merck, Loba, with AR quality 98-99% purity, commercial Gypsum obtained from FCI Aravali Gypsum & Minerals India Ltd. (FAGMIL), Jodhpur, India, nanosilica prepare from the rice husk in the laboratory, Clay (river alluvium) collected from the Kollur, Andhra Pradesh, India. Laboratory made double distilled water with pH 7.02 was used for all mixing and processing steps to prevent chemical interference. All raw materials were stored in airtight containers to avoid contamination and moisture absorption prior to experimentation. The equipment used in this research includes a 100-mesh sieve, analytical balance, oven, furnace, blender, melding tool, and compression test for compressive strength testing.

2.1 Synthesis of SiO_2 Nanoparticle

The rice husk sample (Figure 1) was washed, sun-dried, crushed, and sieved to −80 + 100 mesh, after which 6 g was collected. The husk was treated with 100 mL of 5% (w/v) citric acid and stirred at 80℃ for 20 min, followed by filtration and washing with demineralized water. The material was oven-dried at 110℃ for 24 h and incinerated at 750℃ for 5 h. Subsequently, 1 g of rice husk ash was reacted with 50 mL of 2.5 M NaOH at 100℃ for 1 h to obtain sodium silicate, which was filtered using Whatman No. 42 paper. Ethanol and concentrated H_2SO_4 were added until pH 2 was reached, and the solution was aged for 7 days. The pH was then adjusted to 8 using NH_3, stirred for 2 h, and centrifuged at 6000 rpm for 15 min [14].

The resulting nanosilica gel was dried at 110℃ for 24 h, ground, treated with 1 M HCl for 5 min, and re-dried at 110℃ for 24 h. The final silica nanoparticles were ground and designated as Silica Nanoparticles (SNPs). Characterization was performed using Ultraviolet–visible spectroscopy (UV–Vis), XRD, XRF, Fourier transform infrared spectroscopy (FTIR), SEM–EDS, and zeta potential analysis.

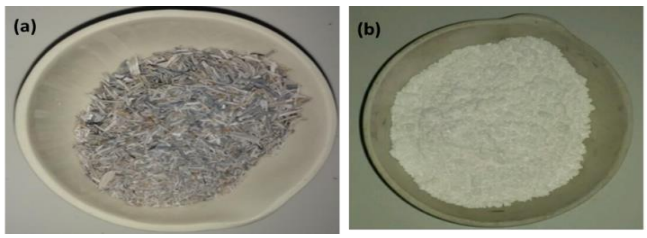

Figure 1. (a) Rice husk; (b) Nanosilica powder

2.2 Preparation of gypsum–nano silica modified fired clay bricks at elevated temperatures

A total of 100 brick specimens measuring 190 × 90 × 40 mm were prepared at the brick firing site with variations in Gypsum and SNPs in different proportions replacing part of the clay according to Table 1. The mixing and molding techniques were generally adopted from conventional brick making. Gypsum and SNPs (prepared in the laboratory as above) were mixed manually in the desired proportions with clay in a dry state. After that, water was added to the dry mixture, and manual mixing continued until a homogeneous mixture was achieved. The mixture was then left for 2-3 hours to allow the water to fill the voids and achieve maximum homogeneity. The mixture lumps prepared for brick making were then placed into a 15 HP brick molding machine. The molded wet clay was then cut in groups to sizes of 190 × 90 × 40 mm. Fresh bricks were dried for 7 days in open air under sunlight until they were sufficiently hard to be transported to the firing kiln. After that, the bricks were placed into the firing kiln and fired for three days. The temperature inside the kiln was maintained at 900℃ to 1100℃. After 20 days, the fired clay bricks were removed from the kiln [15].

Table 1. Composition and processing details of gypsum–silica clay brick samples

Sample ID	Clay (%)	Gypsum (%)	SNPs (%)	Description	Firing Temperatures (℃)
R (G0–S0)	100	0	0	Reference sample with no additives	900, 1000, 1100
G5-S0	95	5	0	Clay with 5% gypsum only	900, 1000, 1100
G5-S5	90	5	5	Clay with 5% gypsum + 5% nano silica	900, 1000, 1100
G5-S10	85	5	10	Clay with 5% gypsum + 10% nano silica	900, 1000, 1100

Table 2. Characterization techniques, instruments, and purposes

Technique	Brand / Model	Purpose
X-ray diffraction (XRD) analysis	Bruker D8 Advance	Phase identification and crystallinity analysis
Ultraviolet–visible spectroscopy (UV–Vis)	Shimadzu UV-2600	Optical absorbance and silica purity verification
Fourier transform infrared spectroscopy (FTIR)	PerkinElmer Spectrum Two	Functional group and bond structure analysis
Thermogravimetric analysis/ derivative differential thermal analysis (TG/drDTG)	Netzsch STA 449 F3	Thermal stability and decomposition behavior
Scanning electron microscopy with energy-dispersive X-ray spectroscopy (SEM–EDS)	JEOL JSM-IT500	Surface morphology and elemental composition
X-ray fluorescence (XRF)	PANalytical Axios	Bulk oxide composition analysis
Dynamic light scattering (DLS) & Zeta Potential	Malvern Zetasizer Nano ZS	Particle size distribution of nano silica & Surface charge and dispersion stability of nano silica

2.3 Characterization of nanosilica and gypsum-silica clay bricks

Characterization of nano silica and gypsum–silica clay bricks was performed using advanced analytical instruments, and the corresponding equipment details and purposes are summarized in Table 2.

Thermomechanical properties were testes according to ASTM procedures like Water Absorption & Apparent Density (ASTM C67), Visual Properties & Dimensions (ASTM C216) and Firing Temp (°C), Bulk Density (g/cm³), Water Absorption (WA) (%), Compressive Strength (MPa), Modulus of Rupture /Flexural Strength/(MPa), Thermal Conductivity (W/m·K) and Linear Shrinkage (LS) (%).

3. RESULTS AND DISCUSSION

3.1 Characterization of synthesized Silica Nanoparticles

Figure 2 presents the SEM image of the SNPs along with the corresponding particle size histogram. The nanoparticles exhibit a predominantly spherical morphology with nanometric dimensions. The histogram indicates an average particle diameter of 127.1 ± 18.6 nm, demonstrating a narrow size distribution. The calculated dispersion of 11.8% is slightly higher than that reported for pure silica, yet still indicates good size uniformity. The EDS spectrum (Figure 3) confirms the elemental composition of the nanoparticles, with silicon and oxygen as the dominant elements. Quantitative analysis reveals weight percentages of 47.99% for Si and 52.01% for O, and atomic percentages of 32.4% and 67.6%, respectively, confirming a near-stoichiometric SiO_2 composition.

The DLS results of the synthesized SNPs are shown in Figure 4. The size distribution exhibits an average hydrodynamic diameter of 128.5 nm with a standard deviation of 37.79 nm. Although slight differences exist between SEM and DLS values, both measurements fall within the acceptable margin of error. This variation is attributed to the hydrodynamic nature of DLS measurements, which account for surface-bound organic species. Figure 5 shows the zeta (ζ) potential of the SNPs, with a measured surface charge of −32.5 mV. This negative charge arises from hydroxyl (–OH) groups on the silanol-rich nanoparticle surface [14]. Zeta potential values equal to or exceeding ±30 mV indicate good colloidal stability, which is consistent with reported standards for stable dispersions [15]. All measurements were performed in triplicate to ensure reliability.

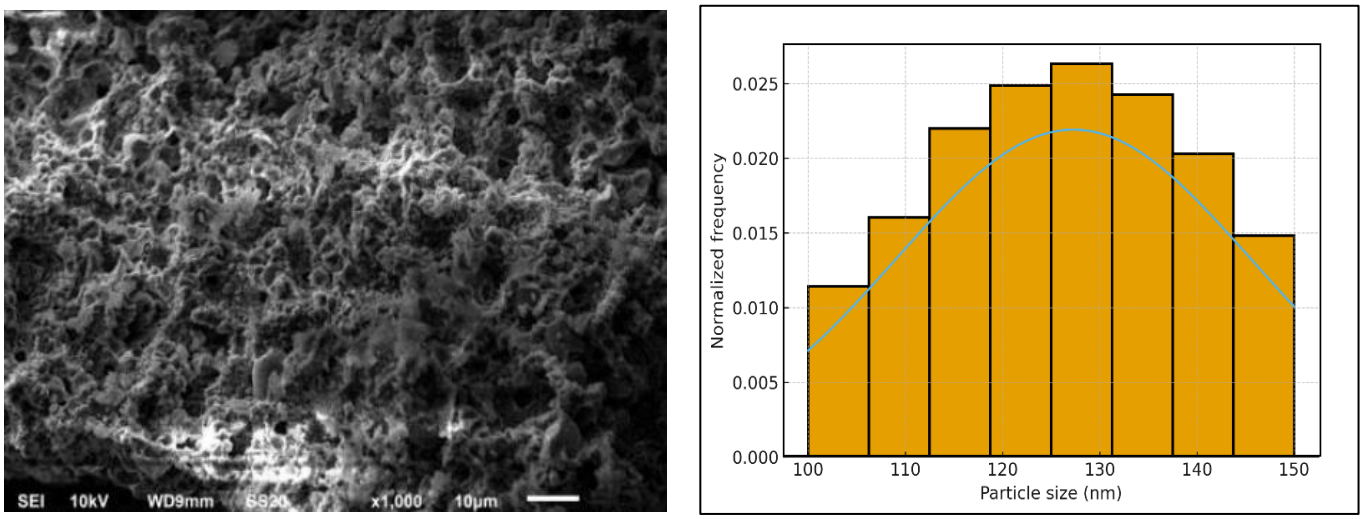

Figure 2. Scanning electron microscopy image SNPs (left) and corresponding particle size histogram (right)

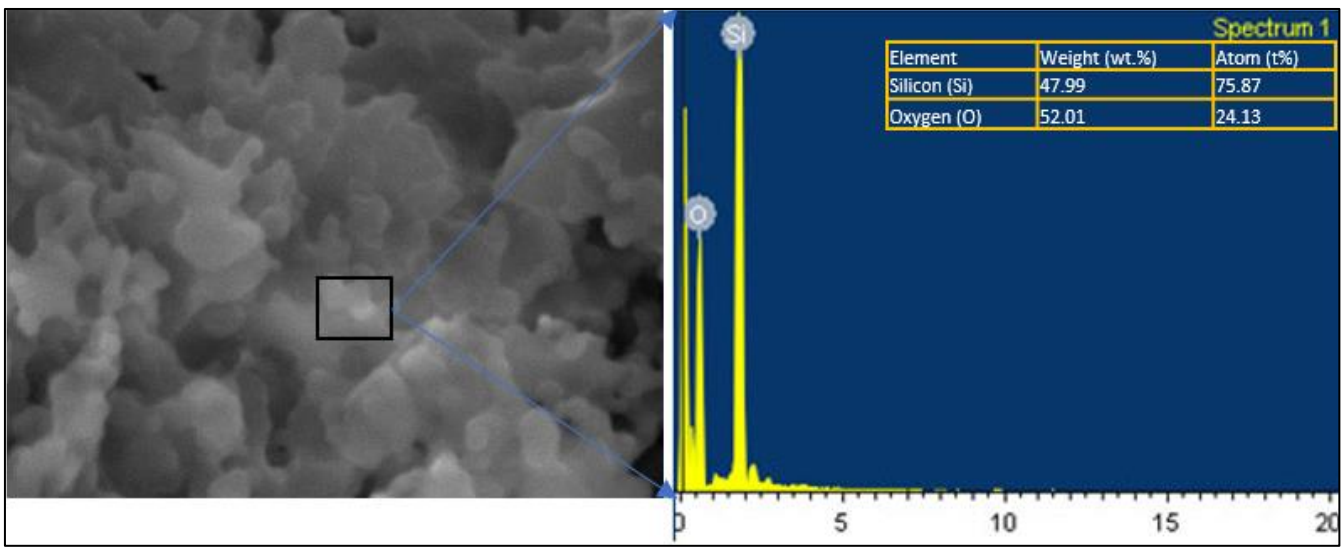

Figure 3. Scanning electron microscopy with energy-dispersive X-ray spectroscopy (SEM–EDS) image SNPs

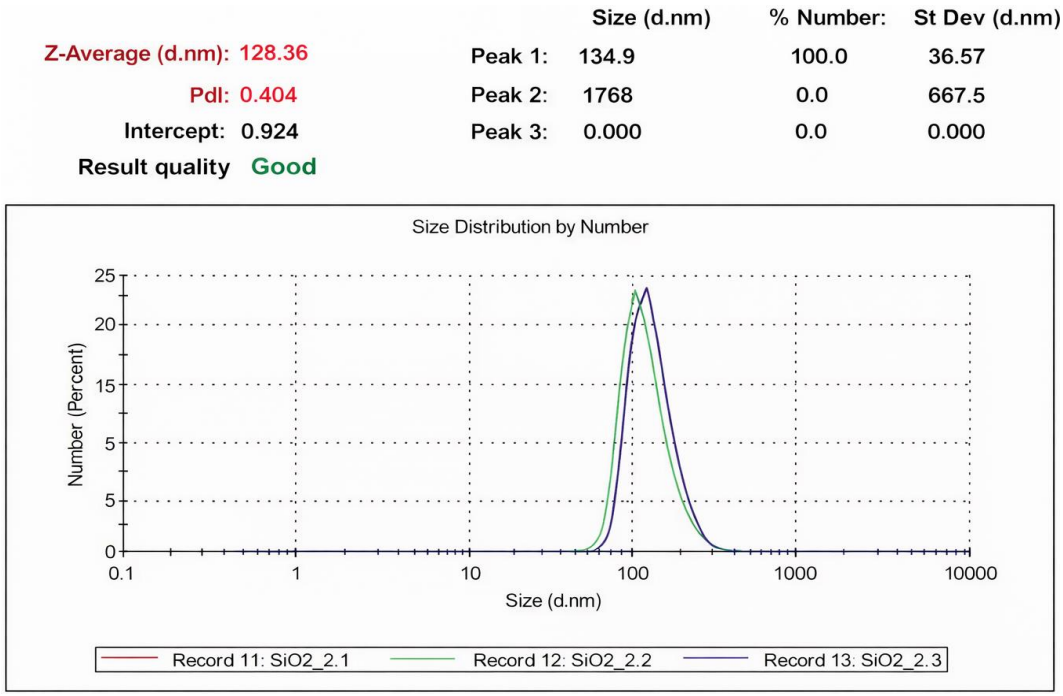

Figure 4. Dynamic light scattering (DLS) spectra of SNPs

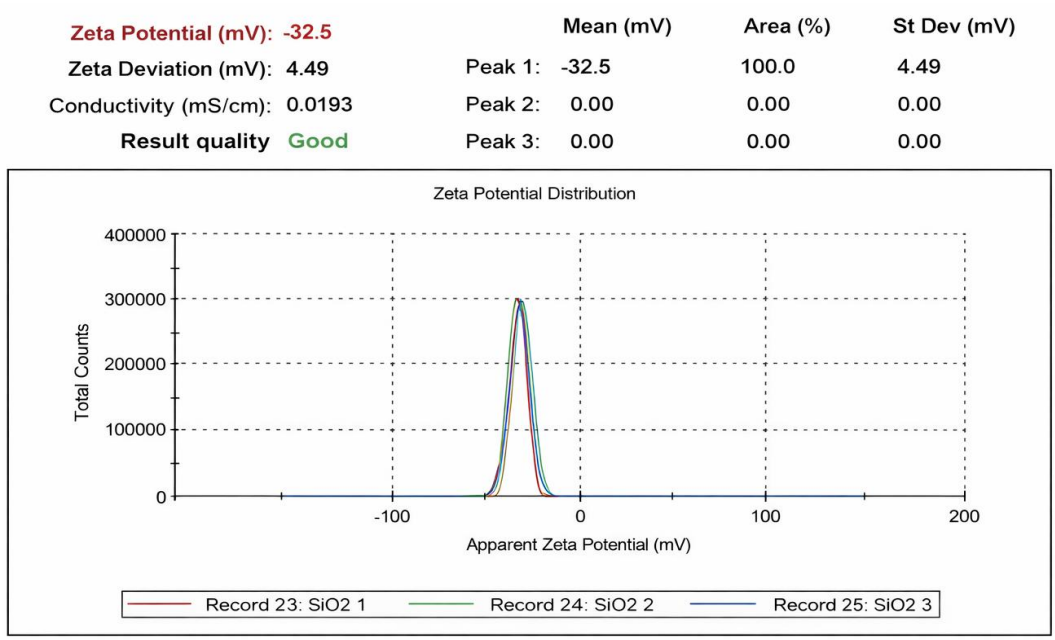

Figure 5. Zeta potential measurement of SNPs

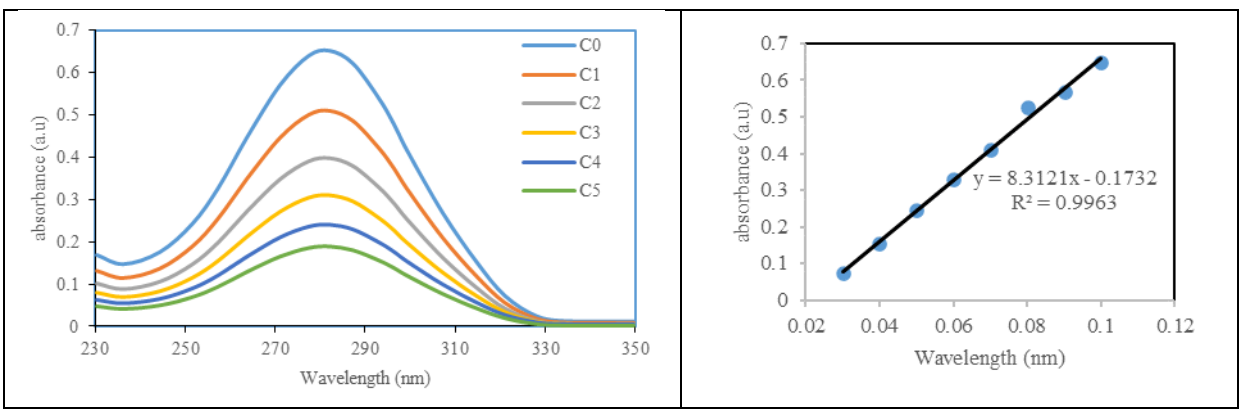

Figure 6. Absorption at 282.1 nm of SNPs (left); Calibration curve constructed from the absorption data (right)

Despite the favorable zeta potential, the SNP suspension exhibited limited colloidal stability, with visible precipitation occurring within a few minutes. Figure 6 illustrates the UV–Vis absorption spectra of SNP solutions at different concentrations. The absorption maximum at 282.1 nm was used to construct the corresponding calibration curve, also shown in Figure 6.

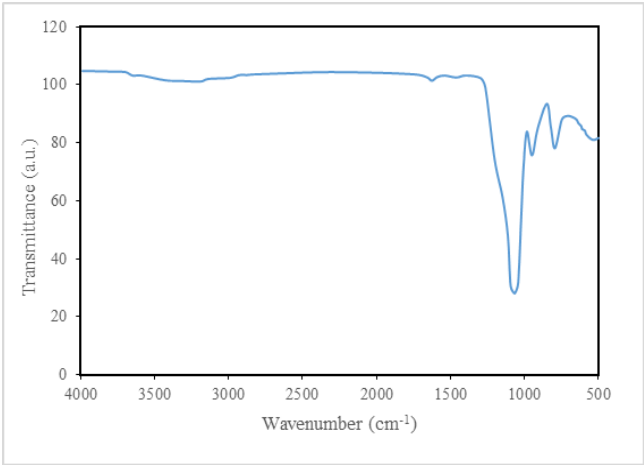

Figure 7. Fourier transform infrared spectroscopy of SNPs and its characteristic absorption peaks

Figure 7 presents the infrared spectroscopy of the SNPs. The image shows the vibrations corresponding to silanol and siloxane groups that confirm the presence of silicon; 795, 950, and 1072 cm^{-1} [16]. Vibrations related to water adsorbed in the sample (1632 and ~3300 cm^{-1}) and some organic residue from the nanoparticle synthesis [17] are also present.

In this study, the XRD test was used to determine the crystal structure, crystal lattice parameters, phase, crystal size of silica, and the elements and compounds contained in the synthesized silica sample. The diffractogram analysis process used Match software to match the obtained data with X-ray diffraction standards for materials [18]. These X-ray diffraction standards are called The Joint Committee on Powder Diffraction Standards (JCPDS/ 29-0085) Based on Figure 8, nanosilica particle with a crystalline structure was obtained. There is Si present at various angles, with the highest intensity peak at 28.33° which corresponds to the silicon phase, has a lattice parameter a = 5.4410 Å, a cubic structure, and a crystal size of 127.6923 nm [18]. Furthermore, SiO_2 is also present at various angles. These peaks correspond to the stishovite phase, with lattice parameters a = 4.1605 Å, b = 4.1294 Å, c = 7.4211 Å, β = 101.375°, and a monoclinic structure. One of these peaks has high intensity, specifically the peak at 31.47° and the peak at 45.20°. At the 31.47° angle, the crystal size is 122.6124 nm, while at the 45.20° angle, the crystal size is 131.1275 nm.

X-Ray Fluorescence (XRF) analysis technique is a technique for analysing a material using a spectrometer equipment emitted by samples from X-ray irradiation. The results of the analysis are given in Table 3.

The SNP contributes remarkably high SiO_2 (95.83 wt%), which leads to a progressive rise in the SiO_2 content from the reference clay sample (G0–S0) through the G5–S0, G5–S5, and G5–S10 mixes at all firing temperatures (900–1100°C). Correspondingly, oxides associated with clay, such as Al_2O_3 and Fe_2O_3, decrease proportionally as they are diluted by the added silica and gypsum. Gypsum addition increases CaO and SO_3 contents in G5–S0, G5–S5, and G5–S10 mixes, with SO_3 showing a distinct reduction as temperature increases due to thermal decomposition of gypsum. The incorporation of nano-silica introduces trace elements such as P_2O_5, ZnO, and Rb_2O, which appear only in nano-silica–modified samples (S5 and S10). High-temperature values include small increases (0.5–1.5 wt%) due to SO_3 and H_2O loss, consistent with ceramic firing chemistry. Overall, the composition reflects silica enrichment, dilution of clay oxides, and thermal desulfation in the modified fired bricks [19].

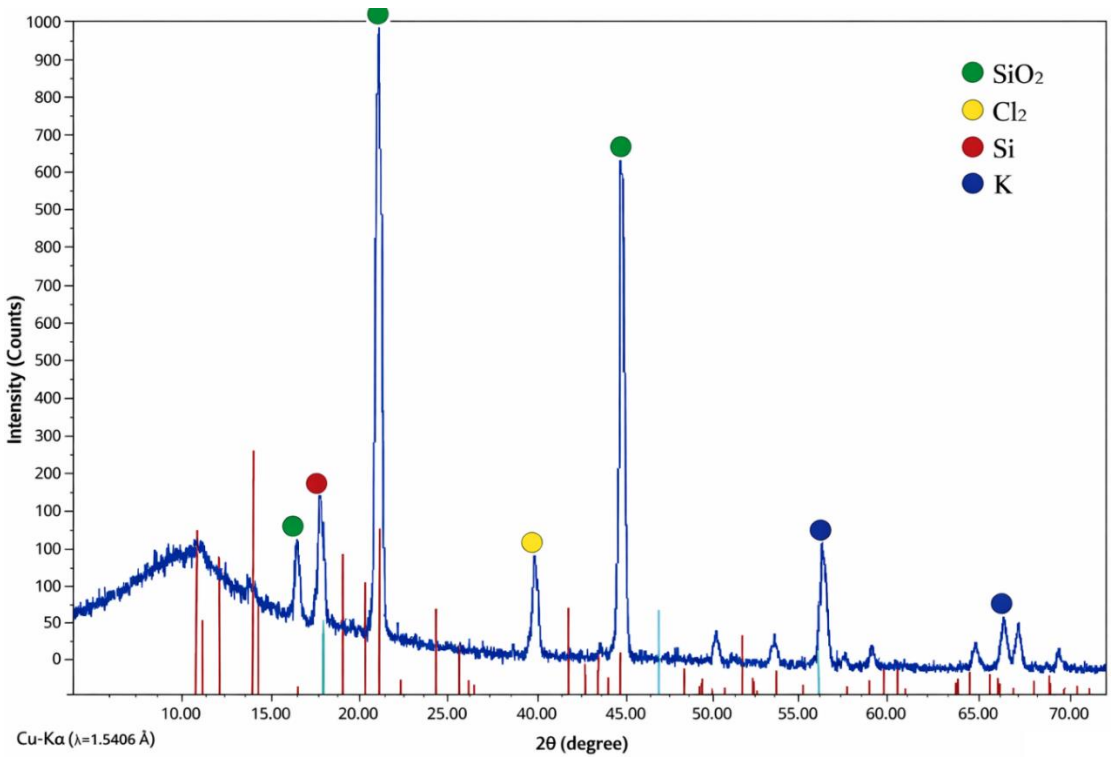

Figure 8. X-ray diffraction of SNP from rice husk

Table 3. XRF analysis of rice husk–based nano-silica, commercial gypsum, and gypsum–nano silica modified fired clay bricks at elevated temperatures

Material / Sample	Oxide Component and Content (wt%)											
	Temp (°C)	SiO_2	Al_2O_3	Fe_2O_3	CaO	MgO	Na_2O	K_2O	SO_3	P_2O_5	ZnO	Rb_2O
Clay	—	55.200	22.800	7.100	3.500	2.400	0.800	2.100	0.600	0.000	0.000	0.000
Nano-silica	—	95.830	0.230	0.120	0.640	0.410	0.090	2.140	0.000	0.060	0.030	0.015
Gypsum	—	4.200	0.600	0.300	32.400	1.100	0.200	0.100	44.800	0.000	0.000	0.000
R (G0–S0)	900	55.200	22.800	7.100	3.500	2.400	0.800	2.100	0.000	0.000	0.000	0.000
	1000	55.800	22.800	7.100	3.500	2.400	0.800	2.100	0.000	0.000	0.000	0.000
	1100	56.400	22.800	7.100	3.500	2.400	0.800	2.100	0.000	0.000	0.000	0.000
G5–S0	900	52.650	21.690	6.760	4.945	2.335	0.770	2.000	2.810	0.000	0.000	0.000
	1000	53.250	21.690	6.760	4.945	2.335	0.770	2.000	1.264	0.000	0.000	0.000
	1100	53.850	21.690	6.760	4.945	2.335	0.770	2.000	0.281	0.000	0.000	0.000
G5–S5	900	54.682	20.562	6.411	4.802	2.236	0.735	2.002	2.780	0.003	0.002	0.002
	1000	55.282	20.562	6.411	4.802	2.236	0.735	2.002	1.251	0.003	0.002	0.002
	1100	55.882	20.562	6.411	4.802	2.236	0.735	2.002	0.278	0.003	0.002	0.002
G5–S10	900	56.713	19.433	6.062	4.659	2.136	0.699	2.004	2.750	0.006	0.003	0.003
	1000	57.313	19.433	6.062	4.659	2.136	0.699	2.004	1.238	0.006	0.003	0.003
	1100	57.913	19.433	6.062	4.659	2.136	0.699	2.004	0.275	0.006	0.003	0.003

3.2 Characterization of fired clay brick samples

Thermomechanical Properties: The specimens were evaluated for their physical and mechanical properties in accordance with ASTM-2018 standards after firing [20]. The tests included Linear Shrinkage (LS), Water Absorption (WA), Apparent Porosity (AP), Bulk Density (BD), and Modulus of Rupture (MOR). Four brick compositions were investigated, and the results are summarized in Table 4. For each composition, five specimens were prepared and fired at 900°C, 1000°C, and 1100°C, resulting in a total of 60 samples. The physico-mechanical properties of the gypsum–nano silica modified fired clay bricks are presented in Table 4.

Linear shrinkage varied systematically with nanosilica content and firing temperature. For all mixtures, shrinkage increased with increasing temperature, with the highest values observed at 1100°C. This trend is primarily attributed to enhanced sintering and vitrification of the ceramic bodies at elevated temperatures. Although linear shrinkage is not standardized under Indian Standards (BIS), it remains an important industrial parameter for ceramic classification. Porous ceramics typically exhibit shrinkage values of ~3%, semi-porous ceramics 4–6%, and vitrified ceramics around 8%. Based on these criteria, the studied bricks fall largely within the semi-porous category.

As shown in Table 4, water absorption decreased with increasing firing temperature, reflecting improved densification of the brick matrix. An inverse relationship was also observed between nanosilica content and water absorption, indicating that nanosilica contributes to pore refinement. The obtained water absorption values are suitable for red ceramic applications. Water absorption and bulk density are closely interrelated; higher firing temperatures promote grain growth, stronger interparticle bonding, and pore filling, thereby reducing water uptake [13].

Apparent porosity, which is directly influenced by firing temperature, showed only minor variation across the tested conditions and correlated well with water absorption and density trends [15]. Increasing nanosilica content did not result in increased porosity at any firing temperature. Instead, specimens containing nanosilica exhibited slightly lower apparent porosity than the reference bricks (R (G0–S0)). Although specimens with nanosilica showed marginally lower bulk density than the reference, higher firing temperatures consistently reduced porosity and water absorption while enhancing overall densification.

The Modulus of Rupture (MOR) generally increased with firing temperature and nanosilica addition, reflecting improved microstructural cohesion due to phase transformations in the clay matrix [21]. At temperatures above 900°C, vitrification occurs through the formation of a liquid glassy phase that fills pores and enhances bonding through capillary action. This process is accompanied by shrinkage and depends strongly on firing temperature, duration, and composition. According to Souza Santos, kaolinite-based ceramics reach maximum firing shrinkage near 950°C, while vitrification occurs between 950°C and 1225°C due to the release of cristobalite (SiO_2) and subsequent glass formation. Despite this, some nanosilica-containing samples showed slightly reduced MOR, likely due to localized phase changes that limited effective particle bonding. Flexural strength values ranged from 2.05 ± 0.016 MPa to 3.05 ± 0.21 MPa, satisfying the ASTM/BSI minimum requirement of ≥ 2.07 MPa for semi-silica and moderately refractory bricks. Comparable or higher MOR values have been reported for clay bricks and bricks incorporating glass waste, perlite waste, or recycled mullite [21-23].

Compressive strength remains a critical parameter for structural applications. The reference brick exhibited the highest compressive strength (35 MPa). With increasing nanosilica content, compressive strength gradually decreased due to increased pore volume, with the 10% nanosilica specimen approaching the permissible lower limit. However, bricks incorporating both gypsum and nanosilica showed a slower rate of strength reduction, maintaining higher compressive strength than bricks containing nanosilica alone at equivalent replacement levels. Thermal conductivity values measured at room temperature ranged from 0.58 to 0.76 W/m·K, indicating acceptable thermal performance for building applications.

The thermal properties, including thermal conductivity, specific heat, and thermal diffusivity, are presented in Table 4. The incorporation of gypsum alone (G5–S0) reduced density by only 1.63% and increased porosity by 2.82% compared with the reference brick (G0–S0). These minor changes had a negligible effect on thermal conductivity, which is primarily governed by porosity. In this study, thermal conductivity decreased slightly for G5–S0, G5–S5, and G5–S10 relative to G0–S0. The obtained values fall within the typical range reported for conventional bricks (0.39–0.67 W/m·K) and are

consistent with literature data for clay–glass waste bricks (0.54–0.58 W/m·K), marble-sludge-based ecological bricks (0.4–0.54 W/m·K), and pure clay bricks (~0.7 W/m·K).

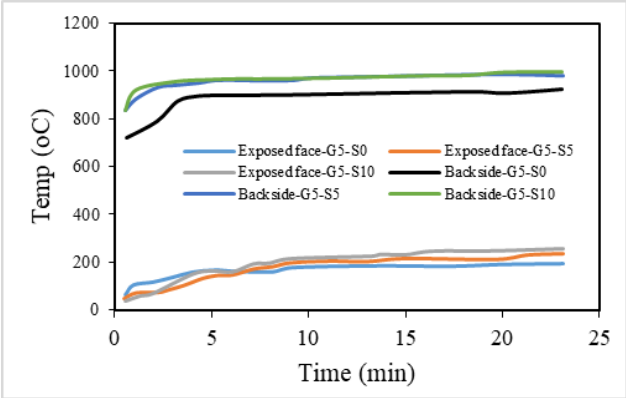

Figure 9. Temperature curves measured in the samples exposed to direct fire using a propane torch

Thermal diffusivity decreased with increasing nanosilica content, with G5–S10 exhibiting a lower value than the reference G5–S0. This indicates that heat propagation was approximately 21% slower due to nanosilica incorporation, resulting in improved insulation performance. As reported in the literature, thermal conductivity and insulation capacity are strongly influenced by porosity characteristics, including pore type (open or closed), size, and uniformity of distribution.

Temperature–time curves obtained under direct flame exposure are shown in Figure 9. During the initial 5 minutes, all samples exhibited rapid heating, followed by temperature stabilization on the exposed surface. Peak temperatures of approximately 950°C were recorded for G5–S0 and G5–S5, while the sample with higher nanosilica content (G5–S10) reached a lower average temperature of about 910°C. On the rear face, temperatures remained below 350°C, corresponding to a thermal gradient of approximately 700°C. Comparable studies on refractory ceramics produced from coal ash waste reported insulation levels of ~500°C over 25 minutes, while kaolinite–mullite ceramics achieved thermal gradients of ~600°C during 30-minute tests. Gypsum–nanosilica composites are known to withstand temperatures up to 1700°C and exhibit good resistance to direct flame exposure, confirming their suitability as thermally insulating and refractory construction materials.

Table 4. Thermo-mechanical properties of gypsum–nano silica modified fired clay bricks at elevated temperatures

Sample ID	Firing Temp (°C)	Bulk Density (g/cm³)	Water Absorption (WA) (%)	Compressive Strength (MPa)	Modulus of Rupture /Flexural Strength/(MPa)	Thermal Conductivity (W/m·K)	Linear Shrinkage (LS) (%)
R (G0–S0)	900	1.58	18.5	35.0	2.10	0.68	2.1
	1000	1.62	17.2	32.8	2.32	0.72	3.0
	1100	1.67	15.8	30.4	2.50	0.76	4.2
G5–S0	900	1.55	19.8	31.6	2.05	0.65	1.9
	1000	1.60	18.1	29.9	2.25	0.70	2.7
	1100	1.65	16.3	27.6	2.40	0.74	3.8
G5–S5	900	1.63	17.2	26.5	2.35	0.60	1.6
	1000	1.68	15.6	23.8	2.58	0.64	2.5
	1100	1.73	14.1	20.4	2.82	0.68	3.3
G5–S10	900	1.66	16.8	17.9	2.48	0.58	1.4
	1000	1.72	15.0	15.5	2.76	0.62	2.1
	1100	1.78	13.6	12.8	3.05	0.66	3.0

With the thermal conductivity results and the temperature record during direct fire exposure, the heat flow graph for G5-S0 and G5-S10 is shown in Figure 10. From the heat flow results, three stages can be highlighted. The initial stage, which lasts approximately the first five minutes of the test, where the temperature is maintained below 200°C. Subsequently, in stage two, from 5 to 10 minutes, the heat transfer begins to decrease for G5-S0 but remains constant for G5-S10. The last stage, after 10 minutes, is considered to be when temperature stabilization is reached. In the case of G5-S10, the heat transfer during the total test time was lower than that recorded for G5-S0. The heat flow in this study is slightly higher than that reported for ceramics from kaolin-mullite, who obtained heat flows between 2.3 and 3.8 J [24]. In this study, the samples were thicker and also more porous than the samples used.

In Figure 11, the marks left on bricks G5-S0, G5-S5, and G5-S10 by direct contact with fire are observed. For G5-S0, the mark is much larger and darker, which infers that there is a greater degree of deterioration in the piece, while in the mark for samples with gypsum and nanosilica G5-S5 and G5-S10, it is observed that the higher the nanosilica content, the smaller the mark. When the test ended, it was observed that the G5-S0 piece had cracked. The better thermal performance in the samples with gypsum and nanosilica is attributed to the existence of phases such as mullite, anorthite, gehlenite, wollastonite and cristobalite with refractory properties previously found in the XRD for sample G5-S10.

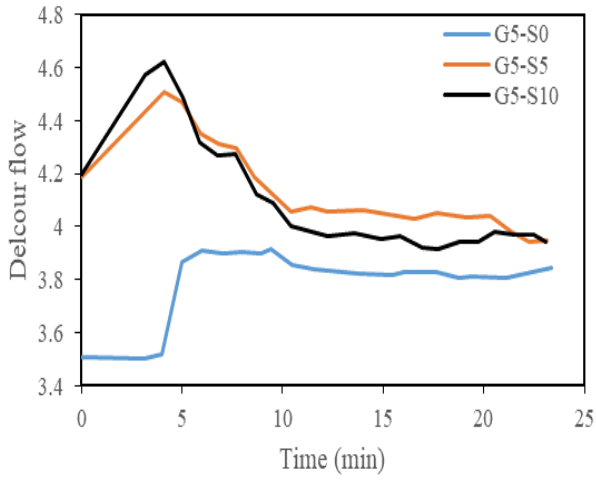

Figure 10. Heat transfer of samples directly exposed to fire with the thermal conductivity results and the temperature

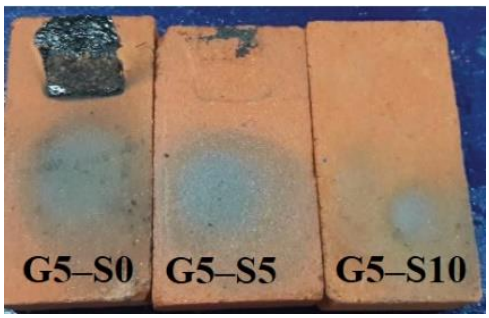

Figure 11. Samples after the flame resistance test

Microstructural and Phase characterization: After completing the compressive strength test, the remaining fragments of the crushed brick samples were taken to observe the morphology or grain size of the samples. The samples were tested using a Scanning Electron Microscope. The samples taken were in the form of fine grains, as the SEM can only accommodate samples measuring 1 mm. The grain size of the brick samples at 1100°C was determined at 2000x magnification, and the grain size was calculated for comparison. This can be seen in Figure 12. Examination of the figures reveals crystalline structures and pore formations, which were also detected in the XRD analyses.

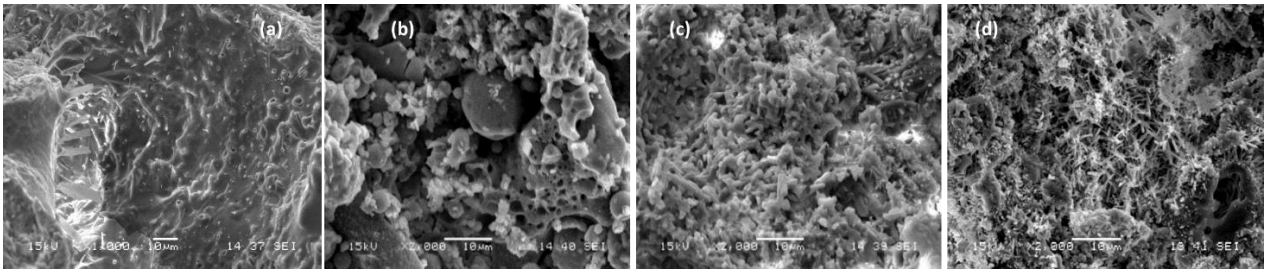

Figure 12. SEM images of produced samples: (a) Reference brick [R (G0–S0)], (b) G5–S0 brick, (c) G5–S5 brick, (d) G5–S10 brick in particular, the brick body with nanosilica addition has a microporous structure due to the hollow spherical shapes of the nanosilica

Figure 12 (G5–S5 and G5–S10) shows spherical nanosilica particles uniformly distributed within the brick matrix, appearing at the microscale. In the fired specimens sintered at 1100°C, the pore sizes are predominantly below 50 µm, with most pores measuring less than 10 µm.

As the gypsum and nanosilica content increases, a pronounced fluxing effect is observed, which reduces melt viscosity and enhances fluidity during firing. This promotes effective pore filling and a consequent reduction in pore number and size. Moreover, increasing the sintering temperature enhances particle rearrangement and mass transport, resulting in improved densification and further pore refinement.

Energy-dispersive X-ray spectroscopy (EDS) analysis (Figure 13) of the binder regions reveals distinct elemental distributions for all four compositions fired at 1100°C. In the reference sample, silicon and oxygen peaks dominate due to the silicate-rich clay matrix. In contrast, the G5–S0 specimen exhibits a pronounced calcium peak accompanied by a reduced silicon signal, indicating the presence of $CaSO_4$ derived from gypsum addition. For nanosilica-doped samples (Si 5% and 10%) combined with 5% gypsum, higher silicon concentrations are detected alongside strong calcium signals. This confirms the coexistence of $CaSO_4$ and nanosilica phases and the formation of a composite microstructure.

These microstructural and compositional observations provide a clear basis for correlating the physicochemical characteristics with the enhanced mechanical performance observed in the gypsum–nanosilica modified brick samples.

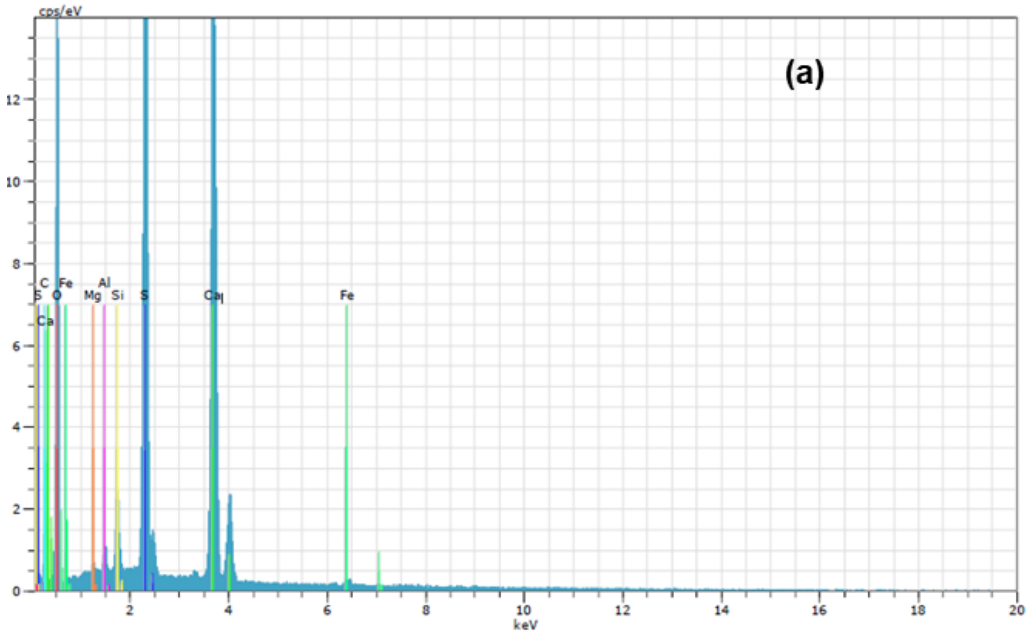

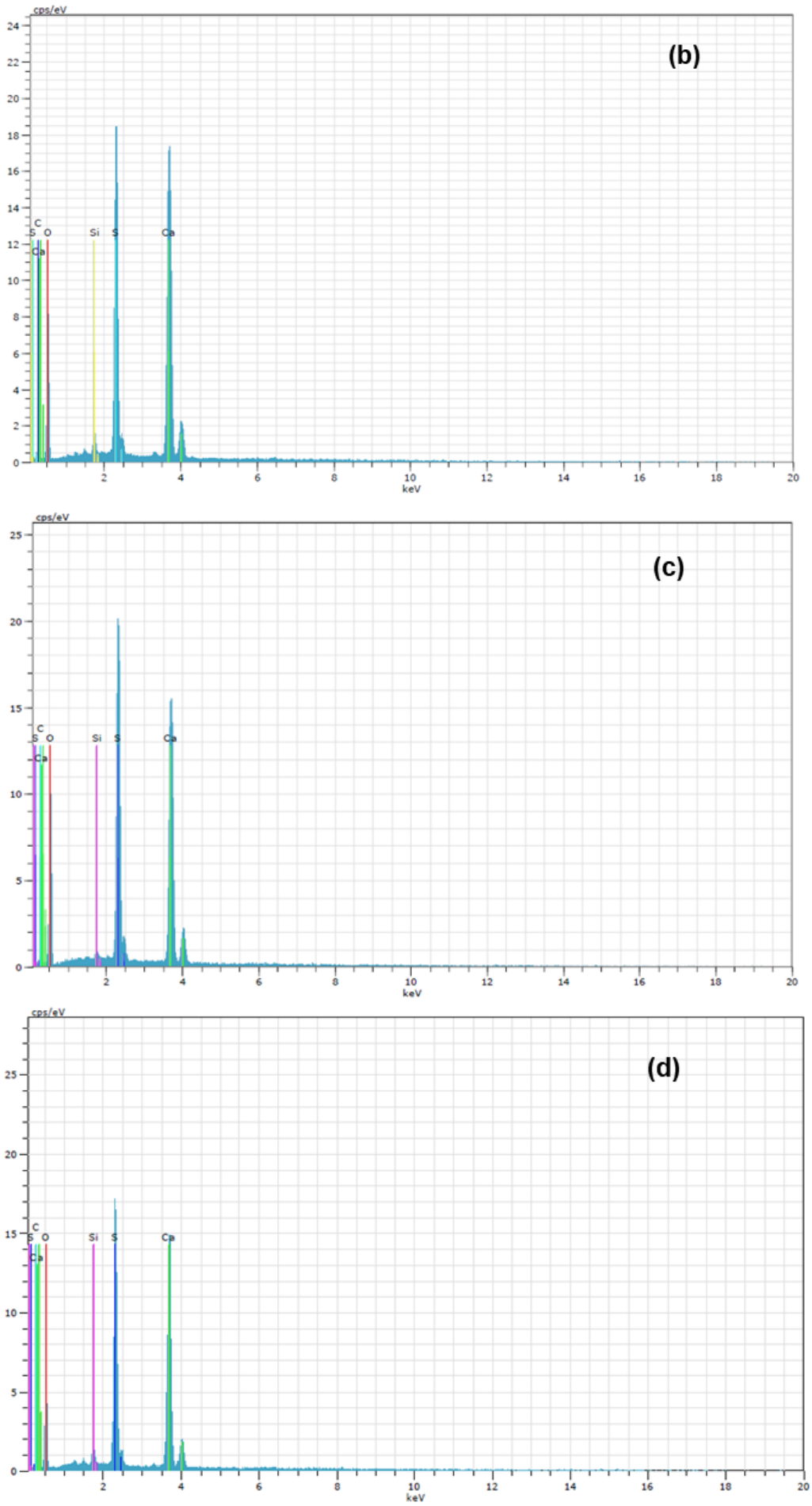

Figure 13. EDS analysis of the produced samples: (a) Reference brick [R (G0–S0)], (b) G5–S0 brick, (c) G5–S5 brick, (d) G5–S10 brick

Suction: Regarding the suction test, the results obtained from the laboratory tests (Table 5) were analysed and processed in order to obtain the variance, standard deviation and coefficient of variation for the standard brick and each of the bricks with substitution percentages in order to obtain statistical data with better understanding and comparison. Regarding the evidence, and based on what was mentioned above with respect to ASTM C62/C216, it shows that the standard bricks have the lowest average suction index (14.14 gr/200cm^2/min) compared to the other controls analysed, being the bricks with the addition of 10% of nanosilica who presented the highest suction index (81.835 gr/200cm^2/min) which represents the accelerated process of water suction during settling. Percentages of addition similar to those in this research resulted in significant improvements in compressive strength. According to the National Building Code of India (NBC) [25], bricks containing gypsum and nanosilica significantly outperformed standard bricks in terms of suction characteristics, with a value of 14.138 gr/200cm^2/min. These bricks were categorized as type I bricks.

Table 5. Suction of masonry units

Mixture Design	Average Suction (gr/200cm²/min)	Variance	Std. Deviation	Coef. of Variation (%)
G0–S0	14.138	3.89	1.972	13.95
G5–S0	47.475	2.741	1.656	3.487
G5–S5	68.863	31.184	5.584	8.109
G5–S10	81.835	7.954	2.820	3.446

XRD characterization of the fired samples: XRD analyses were used to determine the crystalline phases formed in relation to sintering temperatures and increasing gypsum (0%, 5%) and nanosilica (0%, 5%, 10%) content. Figure 14 shows the XRD graphs of the experimental samples sintered at 1100°C. Examination of the figure reveals that with increasing gypsum and nanosilica addition, the formation of Ca-containing phases begins. In the sample coded A (anorthite: ($CaO{\cdot}Al_2O_3{\cdot}2SiO_2$), M (mullite: $3Al_2O_3\ 2SiO_2$), C (gehlenite ($2CaO{\cdot}Al_2O_3{\cdot}SiO_2$), W (wollastonite: $CaO{\cdot}SiO_2$) phases are present. From the results it was concluded that the prepare brick samples shows chemical compatibility between the clay matrix, gypsum and nanosilica doping. During firing, gypsum experienced dehydration and decomposition, providing CaO that responded with aluminosilicate phases in the clay matrix [26]. At high temperatures, expected chemical reactions are shown below:

$$xAl_2O_3 \cdot SiO_2 + yCaO + SiO_2 \rightarrow yCaO \cdot xAl_2\ O_3 \cdot SiO_2$$

The existence of nanosilica improves silica availability and helps liquid-phase sintering, leading to enhanced compression, density and pore refinement.

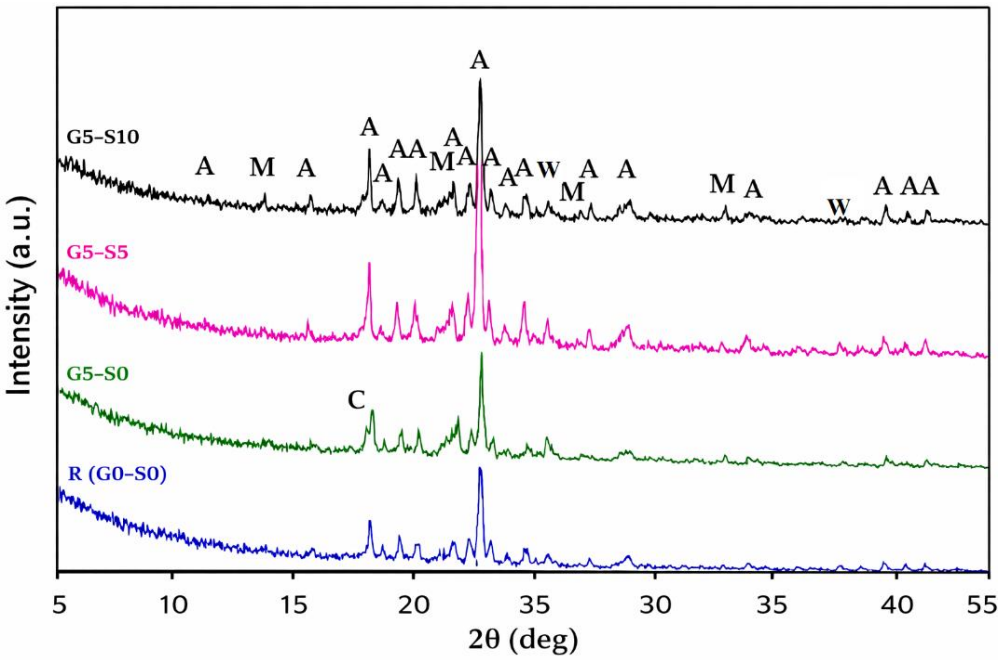

Figure 14. XRD graphs of the produced materials (A: anorthite, M: mullite, C: cristobalite, W: wollastonite)

FT IR analysis of the brick samples: The FTIR spectra (Figure 15) reveal pronounced structural modifications in the brick samples as a function of nanosilica (G) and gypsum (S) concentrations. The broad absorption band in the 3620–3300 cm^{-1} region, along with the peak at approximately 1650 cm^{-1}, corresponds to O–H stretching and H–O–H bending vibrations, respectively, indicating increased hydration and chemically bound water in the G5–S5 and G5–S10 samples [27]. From the image was identified that there a high intense band between 1100 to 1000 cm^{-1}, indicating the Si–O–Si / Si–O–Al Stretching band, by the additive nanosilica increases the silicate frame work in the composition, the peak around 1100 cm^{-1} suggesting improved structural polymerization. The incorporation of nanosilica enhances the silicate framework, as evidenced by the intensification and slight shift of the Si–O–Si stretching bands (1130–1030 cm^{-1}), suggesting

improved structural polymerization [28]. Other peaks and correspond functional groups are listed in the Table 6. From the data it was confirmed the additive may promote the development of complex grouping and modifying the geochemical fingerprint to prepare brick sample.

TGA-DTA analysis: Bricks without additives exhibited moderate thermal resistance (Table 7). The addition of gypsum alone increased porosity and reduced thermal stability due to its thermal decomposition, which hindered the formation of a dense clay matrix.

In contrast, incorporating nanosilica with gypsum significantly improved thermal performance [29]. These bricks developed a higher glassy-phase content with fewer internal microcracks. Nanosilica enhanced melt flow during firing, promoting pore filling and densification, which resulted in improved strength and heat resistance.

Thermogravimetric analysis (TGA) supports these findings. The reference brick showed typical clay behavior, with gradual mass loss up to ~850°C. Gypsum-containing bricks exhibited major decomposition between 750°C and 850°C (Figure 16), with the gypsum-only sample showing rapid weight loss. The inclusion of 5% and 10% nanosilica reduced both the rate and magnitude of mass loss, indicating enhanced thermal stability.

At elevated temperatures, bricks with higher nanosilica content retained more mass, confirming improved resistance to thermal degradation. These results agree with previous studies [5, 6, 10, 30], demonstrating that nanosilica forms a compact, heat-resistant network within the ceramic matrix. Overall, nanosilica effectively offsets the adverse thermal effects of gypsum, and its concentration plays a critical role in optimizing the thermal performance of gypsum–clay composite bricks.

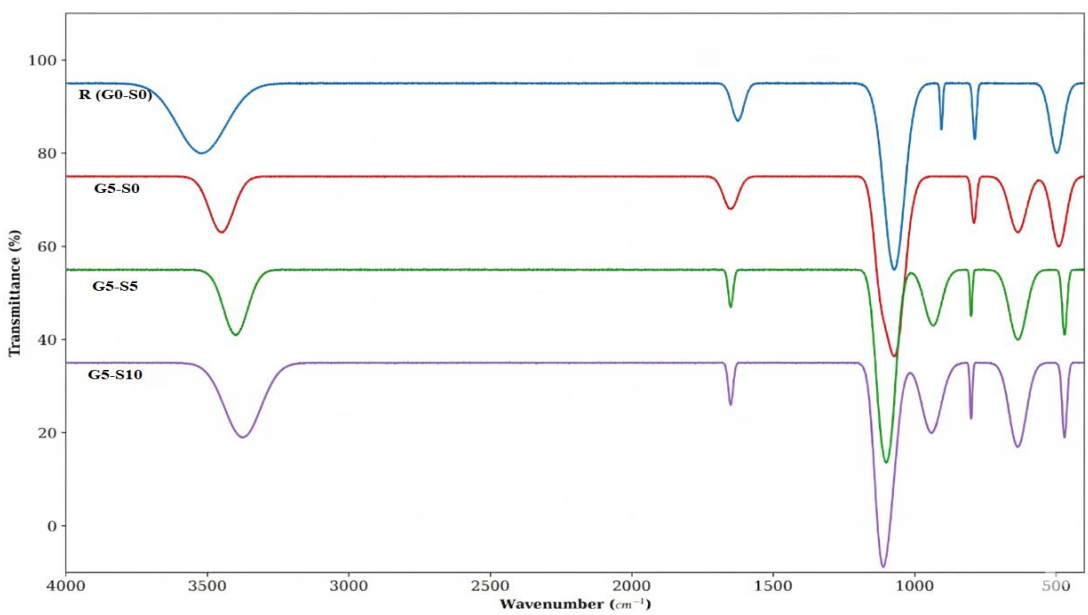

Figure 15. FTIR spectra of 4 brick samples calcined at 1100°C

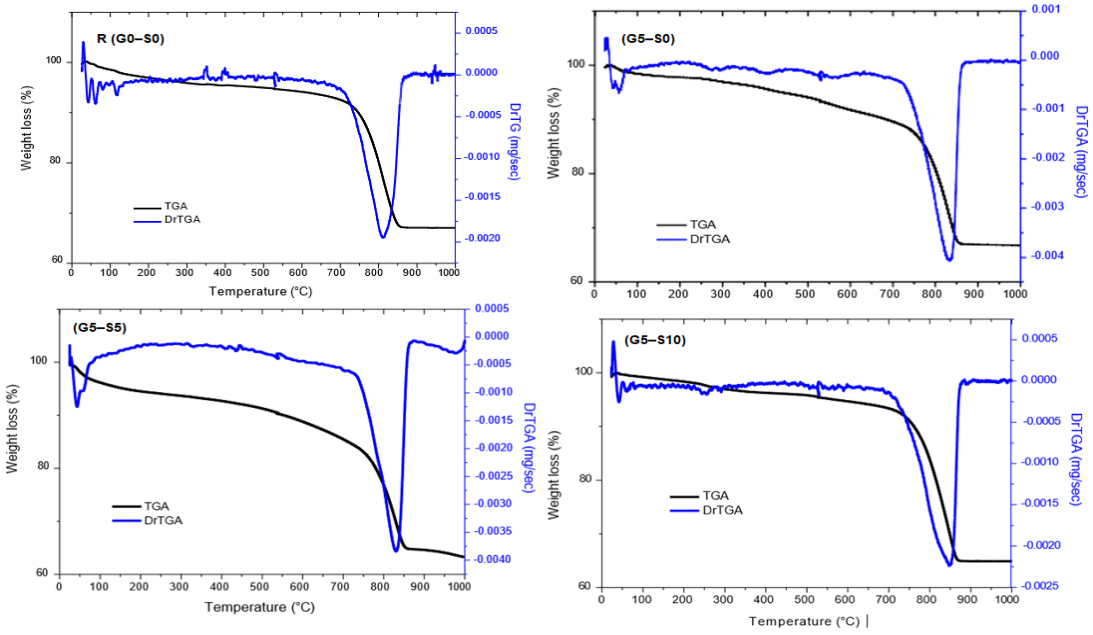

Figure 16. Thermogravimetric analysis coupled with derivative differential thermal analysis (TGA-drDTA) plots for the gypsum–nano silica modified fired bricks (at 1100°C)

Table 6. FTIR functional groups and corresponding frequencies for gypsum–nano silica modified clay bricks

Functional Group / Phase	Brick Samples with Frequencies in cm^{-1}			
	R (G0–S0)	G5–S0	G5–S5	G5–S10
O–H Stretching	3620–3420	3500–3400	3450–3350	3450–3300
H–O–H Bending (Water)	1650–1600	1680–1620	1650	1650
Si–O–Si / Si–O–Al Stretching	1115–1030	1110–1030	1120–1060	1130–1060
Si–OH / Al–OH	910–900	—	970–900	980–900
SO_4^{2-} (Gypsum Sulphate)	—	1150–1100	1150–1100	1150–1100
Ca–SO_4	—	670–600	670–600	670–600
Quartz (Si–O)	795–780	800–780	800	800
Silicate Bending (Si–O–Si / Al–O)	525–470	520–460	470	470

Table 7. Thermal degradation, mass loss, and microstructural characteristics of gypsum–nano silica modified clay bricks

Sample ID	Firing Temp (°C)	Weight Loss (%)	Apparent Porosity (%)	Open Porosity (%)	Glass Phase (%)	Microcrack Density (cracks/mm²)
R (G0–S0)	900	8.4	23.1	18.5	12	6.8
	1000	9.8	20.4	17.2	18	5.2
	1100	11.2	18.0	15.9	25	4.4
G5–S0	900	10.6	24.6	19.8	10	7.1
	1000	12.3	21.8	18.1	16	5.6
	1100	13.8	19.2	16.3	23	4.9
G5–S5	900	9.7	21.4	17.2	22	5.1
	1000	11.0	18.6	15.6	30	3.9
	1100	12.5	16.5	14.1	38	3.2
G5–S10	900	9.2	20.8	16.8	27	4.8
	1000	10.5	18.1	15.0	35	3.5
	1100	11.8	15.9	13.6	45	2.8

4. CONCLUSIONS

This study shows that using both gypsum and nanosilica in clay bricks changes their structure and properties. Adding nanosilica generally improves brick quality compared to standard ones. Tests on fired bricks measured shrinkage, water absorption, porosity, density, and strength. Higher nanosilica amounts affect the brick's internal structure. During firing, gypsum creates pores as it breaks down. Nanosilica, however, helps fill and refine these pores. Bricks with more nanosilica have a denser structure with fewer connected pores, which leads to better bending strength; their compressive strength slightly decreased due to the changed microstructure. Thermal conductivity increased slightly with temperature, a sign of lower porosity and stronger bonds. Nanosilica from agricultural sources, when mixed with gypsum, makes the brick more resistant to heat. In a direct fire test, the brick with the most nanosilica (G5-S10) performed best. It transferred less heat, left a smaller burn mark, and did not crack, unlike the brick with gypsum alone, which cracked

ACKNOWLEDGMENT

The author gratefully acknowledges the support of the Ministry of Education, Iraq, and Geniuses High School for Outstanding Students, under the General Directorate of Al-Rusafa the Third, Baghdad, Iraq, for providing the institutional support and facilities necessary to carry out this research.

REFERENCES

[1] Al-Omari, A., Khattab, S. (2021). Characterization of building materials used in the construction of historical Al-Omariya mosque minaret in Mosul's old city, Iraq. Journal of Building Engineering, 33: 101645. https://doi.org/10.1016/j.jobe.2020.101645

[2] Awadh, S.M., Awad, A.M. (2021). Evaluation of the Injana claystone from Central Iraq for the brick industry. Kuwait Journal of Science, 48(2). https://doi.org/10.48129/kjs.v48i2.9006

[3] Hu, J., Ahmed, W., Jiao, D. (2024). A critical review of the technical characteristics of recycled brick powder and its influence on concrete properties. Buildings, 14(11): 3691. https://doi.org/10.3390/buildings14113691

[4] Zhao, Y., Tao, H., Xie, D., Lv, M., Sun, S. (2025). Mechanical properties, durability, and life cycle assessment of recycled brick powder concrete reinforced with different fibers. Case Studies in Construction Materials, 24: e05723. https://doi.org/10.1016/j.cscm.2025.e05723

[5] Alani, A.A.A., Hama, S.M., Jahami, A. (2025). Influence of a nano-dispersed additive from waste brick powder on the structure formation of concrete and heat dissipation characteristic. Construction and Building Materials, 481: 141561. https://doi.org/10.1016/j.conbuildmat.2025.141561

[6] Abir, A.H., Mozumder, A. (2025). Synergistic nanomodification of untreated recycled brick aggregate concrete with nanosilica and graphene oxide in OPC–LC3 binders: Multi-performance optimization and life cycle assessment. Journal of Engineering and Applied Science, 72(1): 127. https://doi.org/10.1186/s44147-025-00700-1

[7] de Castro Carvalho, I., Zhang, Z., Kirchheim, A.P., Costa, H.N., Cabral, A.E. (2025). Waste clay brick utilization in alkali-activated materials: A review on fresh and hardened state properties. Materials Reports: Solidwaste and Ecomaterials, 1: 9520005.

https://doi.org/10.26599/MRSE.2025.9520005
[8] Ali, A., Chiang, Y.W., Santos, R.M. (2022). X-ray diffraction techniques for mineral characterization: A review for engineers of the fundamentals, applications, and research directions. Minerals, 12(2): 205. https://doi.org/10.3390/min12020205
[9] Al-Assadi, F.I., Al-Dewachi, M.H. (2024). The role of brick in determining features of Iraqi architecture. IOP Conference Series: Materials Science and Engineering, 881(1): 012018. https://doi.org/10.1088/1757-899X/881/1/012018
[10] Jenima, J., Priya Dharshini, M., Ajin, M.L., Jebeen Moses, J., Retnam, K.P., Arunachalam, K.P., Avudaiappan, S., Arrue Munoz, R.F. (2024). A comprehensive review of titanium dioxide nanoparticles in cementitious composites. Heliyon, 10(20): e39238. https://doi.org/10.1016/j.heliyon.2024.e39238
[11] Mallik, B., Srivastava, S.K. (2025). Recent development on magnetic properties of MnBi alloys. Next Materials, 10: 10150. https://doi.org/10.1016/j.nxmate.2025.101501
[12] Prabalini, C., Aysha Farsana, Z., Sumathi, A. (2018). Effect of TiO_2 nanoliquid on the properties of cement mortar. International Journal of Engineering and Technology, 7: 223-227. https://doi.org/10.14419/ijet.v7i3.12.16029
[13] Rauta, P.R., Sahoo, N. (2015). Properties enhancement of refractory bricks by incorporation of nanomaterials. In Proceedings of the 2015 International Conference on Nascent Technologies in the Engineering Field (ICNTE), Navi Mumbai, India, pp. 1-6. https://doi.org/10.1109/ICNTE.2015.7029908
[14] Kamboj, R., Bains, A., Sharma, M., Kumar, A., Ali, N., Parvez, M.K., Chawla, P., Sridhar, K. (2024). Green synthesis of rice straw-derived silica nanoparticles by hydrothermal process for antimicrobial properties and effective degradation of dyes. Process Safety and Environmental Protection, 185: 1049-1060. https://doi.org/10.1016/j.psep.2024.03.078
[15] Sütçü, M., Faisal, M.S., Danish, A., Erdogmus, E., Gencel, O., Ozbakkaloglu, T. (2024). Preparation and performance evaluation of waste tuff-modified bricks for sustainable built environment: Effect of firing temperature and molding pressure. Construction and Building Materials, 420: 135438. https://doi.org/10.1016/j.conbuildmat.2024.135438
[16] Al Abboodi, S.M.T., Al Shaibani, E.J.A., Alrubai, E.A. (2020). Preparation and characterization of nano silica prepared by different precipitation methods. IOP Conference Series: Materials Science and Engineering, 978(1): 012031. https://doi.org/10.1088/1757-899X/978/1/012031
[17] Jyoti, A., Singh, R.K., Kumar, N., Aman, A.K., Kar, M. (2021). Synthesis and properties of amorphous nanosilica from rice husk and its composites. Materials Science and Engineering: B, 263: 114871. https://doi.org/10.1016/j.mseb.2020.114871
[18] Patil, N.B., Sharanagouda, H., Doddagoudar, S.R., Ramachandra, C.T., Ramappa, K.T. (2018). Biosynthesis and characterization of silica nanoparticles from rice (Oryza sativa L.) husk. International Journal of Current Microbiology and Applied Sciences, 7(12): 2298-2306. https://doi.org/10.20546/ijcmas.2018.712.261
[19] de Jesus Paula, R., Moreira, C.E.M., Junior, A.T.D., Fagundes, F.G., et al. (2025). Nanosilica from diatomaceous earth waste in the brewing industry with pozzolanic potential. Cleaner Waste Systems, 12: 100362. https://doi.org/10.1016/j.clwas.2025.100362
[20] ASTM International. (2023). Standard test methods for sampling and testing brick and structural clay tile (ASTM C67/C67M-23a). https://standards.iteh.ai/catalog/standards/astm/3dd28e97-bdf2-4c00-b9f9-5c92e91729e0/astm-c67-c67m-23a.
[21] Ngo, V.T., Bui, T.T., Nguyen, T.C.N., Nguyen, T.T.N., Lam, T.Q.K. (2021). Effect of nano-silica content on compressive strength and modulus of elasticity of high-performance concrete. In Proceedings of the 3rd International Conference on Sustainability in Civil Engineering: ICSCE 2020, Hanoi, Vietnam, pp. 153-159. https://doi.org/10.1007/978-981-16-0053-1_19
[22] Blanca, L.N., Nilas, A.Z.A.M.A., Benoit, B.L.A.Y.S.A.T., Rostand, M.P. (2025). Fired clay bricks made by incorporating organic additives: A review. Case Studies in Construction Materials, 23: e05037. https://doi.org/10.1016/j.cscm.2025.e05037
[23] Velasco, P.M., Ortíz, M.M., Giró, M.M., Velasco, L.M. (2014). Fired clay bricks manufactured by adding wastes as sustainable construction material–A review. Construction and Building Materials, 63: 97-107. https://doi.org/10.1016/j.conbuildmat.2014.03.045
[24] Villaquirán-Caicedo, M.A., De Gutiérrez, R.M. (2018). Mechanical and microstructural analysis of geopolymer composites based on metakaolin and recycled silica. Journal of the American Ceramic Society, 102(6): 3653-3662. https://doi.org/10.1111/jace.16208
[25] Bureau of Indian Standards. (2016). National building code of India 2016 (Part 3: Fire and structural safety). BIS. https://www.bis.gov.in/.
[26] Doleželová, M., Scheinherrová, L., Krejsová, J., Vimmrová, A. (2018). Effect of high temperatures on gypsum-based composites. Construction and Building materials, 168: 82-90. https://doi.org/10.1016/j.conbuildmat.2018.02.101
[27] Nirmala, G., Viruthagiri, G. (2014). FT-IR characterization of articulated ceramic bricks with wastes from ceramic industries. Spectrochimica Acta Part A: Molecular and Biomolecular Spectroscopy, 126: 129-134. https://doi.org/10.1016/j.saa.2014.01.143
[28] Singh, S.K., Singh, M. (2020). The mineralogical and physical behavior of brick aggregates in twelfth century brick-lime stepwell plasters of Gandhak-ki-baoli, New Delhi. Journal of Architectural Conservation, 26(2): 184-200. https://doi.org/10.1080/13556207.2020.1768480
[29] Feldthus, F.B., Ottosen, L.M., Kirkelund, G.M., Bertelsen, I.M.G. (2025). Thermogravimetric analysis (TGA) of brick clay and sewage sludge ash. DTU Data. https://doi.org/10.11583/dtu.30157066
[30] Kaika, Y.K., Umaru, I., Idris, M.M., Rilwan, U., Guto, J.A., Sayyed, M., Maisalatee, A., Mundi, A.A., Mahmoud, K. (2025). Microstructural, thermal analysis, and gamma-ray shielding properties of bricks made of various local natural materials. Radiation Physics and Chemistry, 236: 112742. https://doi.org/10.1016/j.radphyschem.2025.112742

NOMENCLATURE

Symbol / Abbreviation	Description
AP	Apparent Porosity (%)
ASTM	American Society for Testing and Materials
BD	Bulk Density (g/cm³)
CaO	Calcium Oxide
$CaSO_4$	Calcium Sulfate (Gypsum)
DLS	Dynamic Light Scattering
EDS	Energy Dispersive X-ray Spectroscopy
FTIR	Fourier Transform Infrared Spectroscopy
G	Gypsum
G0–S0	Reference brick sample without additives
G5–S0	Brick with 5% gypsum
G5–S5	Brick with 5% gypsum and 5% nanosilica
G5–S10	Brick with 5% gypsum and 10% nanosilica
LS	Linear Shrinkage (%)
MOR	Modulus of Rupture (MPa)
NPs	Nanoparticles
SNPs	Silica Nanoparticles
SEM	Scanning Electron Microscope
SEM–EDS	Scanning Electron Microscopy with Energy Dispersive Spectroscopy
SiO_2	Silicon Dioxide (Nanosilica)
TGA	Thermogravimetric Analysis
DTA	Differential Thermal Analysis
TG–DTG	Thermogravimetric–Derivative Thermogravimetric Analysis
UV–Vis	Ultraviolet–Visible Spectroscopy
WA	Water Absorption (%)
XRD	X-ray Diffraction
XRF	X-ray Fluorescence
ζ	Zeta Potential (mV)

Greek symbols

Symbol	Description
α	Thermal Diffusivity (mm²/s)
β	Monoclinic Angle (XRD Analysis) (degrees (°))
Δ	Change / Difference
λ	Thermal Conductivity (W/m·K)
μm	Micrometer (pore size) (μm)
nm	Nanometer (particle size) (nm)
θ	Diffraction Angle (XRD) (degrees (°))
ζ	Zeta Potential (mV)